Bulletin of the Seismological Society of America, Vol. 103, No. 2A, pp. 694–708, April 2013, doi: 10.1785/0120120056

Ⓔ

Kinematic and Dynamic Inversion of the 2008 Northern Iwate Earthquake

by S. Ruiz* and R. Madariaga

Abstract We perform kinematic and dynamic inversion of the 24 July 2008 (M_w 6.8) Northern Iwate intermediate depth earthquake in Japan using strong-motion records from the K-NET and KiK-net networks. The rupture of this moderate magnitude earthquake is modeled as a simple elliptical patch. The optimal solutions are found comparing observed and synthetic records using an L^2 norm and the neighborhood algorithm to search for the best solution, followed by an exploration of solution space with a Monte Carlo technique. The geometry of the rupture, rupture velocity, and slip distribution are estimated by kinematic inversion. The rupture geometry, stress, and friction parameters are obtained by dynamic inversion. Both approaches converge to very similar source models with semiminor axes of 4 km, maximum slip of about 4 m, and large stress drops in the 30–45 MPa range. Rupture duration was less than 3 s because of very high sub-Rayleigh rupture propagation speeds. Energy release rate for the best models was in the range 23–36 MJ/m^2, a rather large value for events of this size. For both kinematic and dynamic inversion we found families of solutions that fit the strong-motion data within a certain error, confirming the strong trade-off among inverted parameters. Finally, we demonstrate that dynamic inversion solutions are controlled by the dynamic similarity parameter κ and by seismic moment M_0. These two parameters define a region of model space where dynamically similar models fit the observations with approximately the same misfit.

Online Material: Figures that compare observed and synthetic waveforms for all available stations and comparison of Fourier spectrum of observed and synthetic seismograms.

Introduction

The Iwate 2008 intraslab intermediate depth (M_w 6.8) earthquake occurred inside the subducted Pacific plate in northern Japan (Japan Meteorological Agency [JMA], Suzuki *et al.*, 2009). The epicenter of the earthquake was located on land so that it had an excellent azimuthal coverage by strong-motion instruments of the K-NET and KiK-net networks. The maximum JMA seismic intensity was 6− and PGA values larger than 1g were observed at a few sites. Strong intermediate earthquakes of this kind occur often in Japan, for instance the 1987 M_{JMA} 6.7 eastern Chiba event (Fukuyama, 1991); the 1993 M_w 7.6 Kushiro-oki event (Ide and Takeo, 1996); the 1994 M_w 8.2 Hokkaido Toho-oki (Shikotan) earthquake (Kikuchi and Kanamori, 1995); the 2001 M_w 6.7 Geiyo earthquake (Miyatake *et al.*, 2004); or the 2003 M 7.1 Miyagi-oki earthquake (Okada and Hasegawa, 2003). Thanks to the dense seismic and strong-motion networks of Japan it is possible to study these events in detail because local site effects are limited for the stations located closer to the epicenter.

The conventional approach to invert seismic ruptures in the near field is to do a kinematic inversion of the observed records in order to compute the distribution of slip or slip rate on the fault for simple models of the rupture process. From these kinematic models of the rupture process it is then possible to compute dynamic source parameters (Fukuyama and Mikumo, 1993; Ide and Takeo, 1996; Bouchon *et al.*, 1998; among others). Many approximations used in the kinematic models affect the determination of the dynamic parameters (Guatteri and Spudich, 2000; Piatanesi *et al.*, 2004), propagating errors from the kinematic inversion to the dynamic simulation. A better method would be to invert directly for stress and strength distribution using fully dynamic models. Dynamic inversion is difficult because we need exceptionally well-recorded events with limited site effects. Dynamic inversion is also expensive because at each step in the inversion

*Also at Laboratoire de Géologie, Centre National de la Recherche Scientifique, École Normale Supérieure, 24 Rue Lhomond, 75231 Paris Cedex 05, France.

process it is necessary to compute a full numerical simulation. The first full dynamic inversions were made by Peyrat and Olsen (2004), DiCarli *et al.* (2010), and Ruiz and Madariaga (2011). In the latter work a full dynamic inversion was made using an elliptical patch approach in which it is assumed that the geometry of the source can be modeled by a small number of elliptical patches. In the inversion of the 2007 Michilla northern Chile earthquake, Ruiz and Madariaga (2011) used only five strong-motion records for the determination of 11 source parameters, among them the stress, friction, and geometrical parameters.

In the present paper we do dynamic inversion of the 2008 Northern Iwate intermediate depth earthquake of northern Japan. This earthquake was recorded by several dozen strong-motion instruments of the K-NET and KiK-net networks. Suzuki *et al.* (2009) studied this earthquake using a classical kinematic inversion method based on rectangular slip patches. Here we model the earthquakes using simple elliptical slip or stress patches in the kinematic and dynamic inversion. We use a neighborhood algorithm (NA) to determine the best fitting models and a Monte Carlo approach (MC) to study the resolution of inversion and to explore the vicinity of the optimal model.

The Iwate 2008 Earthquake and Available Data

The 24 July 2008 Northern Iwate, Japan, intraplate intermediate depth earthquake was located at 39.739° N, 141.670° E, and 115-km depth (National Research Institute for Earth Science and Disaster Prevention, NIED). Its seismic moment was 1.93×10^{19} N·m and it had a normal-fault focal mechanism (strike 178°, dip 73°, and rake −95°) with large non-double-couple component according to the Global Moment Tensor project (GCMT). For reasons of simplicity, however, in our inversions we used a single fault plane and did not consider possible non-double-couple components, nor two different fault planes as was proposed by Suzuki *et al.* (2009). This earthquake was very well recorded by the K-NET (Kinoshita, 1998) and KiK-net strong-motion networks (Aoi *et al.*, 2000), deployed by NIED in Tsukuba and by the Japan Meteorological Agency (JMA; Fig. 1). We used both networks in this work, but from the KiK-net network stations we chose only the strong-motion instruments installed in boreholes. Figure 1 shows the location of the earthquake (star) and the location of the strong-motion instruments that we used in kinematic and dynamic inversion.

Records from both networks were band-pass filtered with a high-pass corner at 0.5 Hz and a variable low-pass corner frequency; we used 0.02 Hz for borehole KiK-net stations and 0.04 Hz for surface K-NET stations. The low frequency cutoff was chosen to avoid the effects of rotation and noise on the integration of strong-motion records. The high-pass limit is necessary to avoid deficiencies in the 1D velocity model available for the region and to reduce site effects. The strong-motion records were filtered using a Butterworth filter of order 2, then they were resampled from 100 Hz to

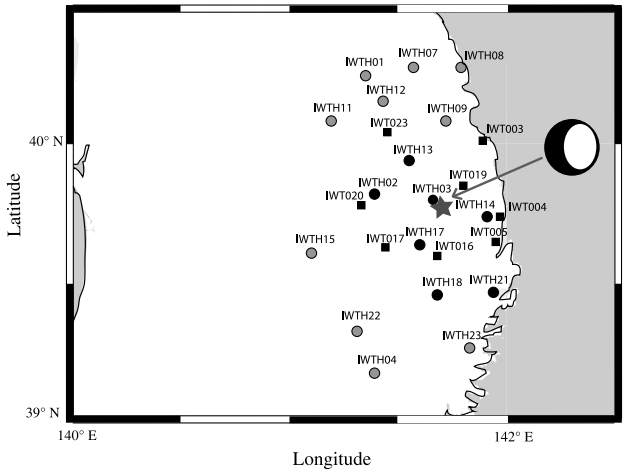

Figure 1. Location and instruments available for the study of the Northern Iwate intermediate depth earthquake of 2008. Star, epicenter; circles, KiK-net stations; squares, K-NET stations. From the KiK-net network we chose only the strong-motion instruments installed in boreholes. Black circles and squares, strong-motion sites located less than 40 km from the epicenter (Dataset 2); gray circles and squares, sites at epicentral distances less than 65 km (Dataset 1).

5 Hz, and twice integrated removing the linear base line in each integration. Figure 2 shows the processing of two records used in the inversion. In panel (a) we compare the Fourier spectra at stations IWTH03 EW and IWT023 EW before and after the application of the band-pass filter. The filter corners are indicated by the vertical lines. The gray trace shows the acceleration Fourier spectra of the original strong-motion record with only a linear base line removed and the black trace shows the filtered acceleration Fourier spectrum. Figure 2b shows the filtered acceleration, velocity, and displacement records at stations IWTH03 EW and IWT023 EW. Inversions were made using displacement because we were interested in determining the low frequency properties of the source, such as the average slip and stress drop. Several velocity records were affected by surface waves that we cannot reproduce with the 1D velocity model that we used. Modeling 2D or 3D wave propagation is currently beyond the computer resources that are available to us.

Kinematic Inversion

We first did a kinematic inversion in order to determine the main features of the models based on the elliptical patch approximation that will be used in the dynamic inversion (see DiCarli *et al.*, 2010; Ruiz and Madariaga, 2011). The shape of the rupture zone is assumed to be an elliptical patch located inside a fault plane of 32×32 km. The geometry of the ellipse is defined by the following parameters: the location of the center of the ellipse with respect to the hypocenter of the earthquake, the principal semi-axes (noted a and b), and the angle of the principal axis with respect to the horizontal. We assumed also that the slip distribution had a Gaussian distribution

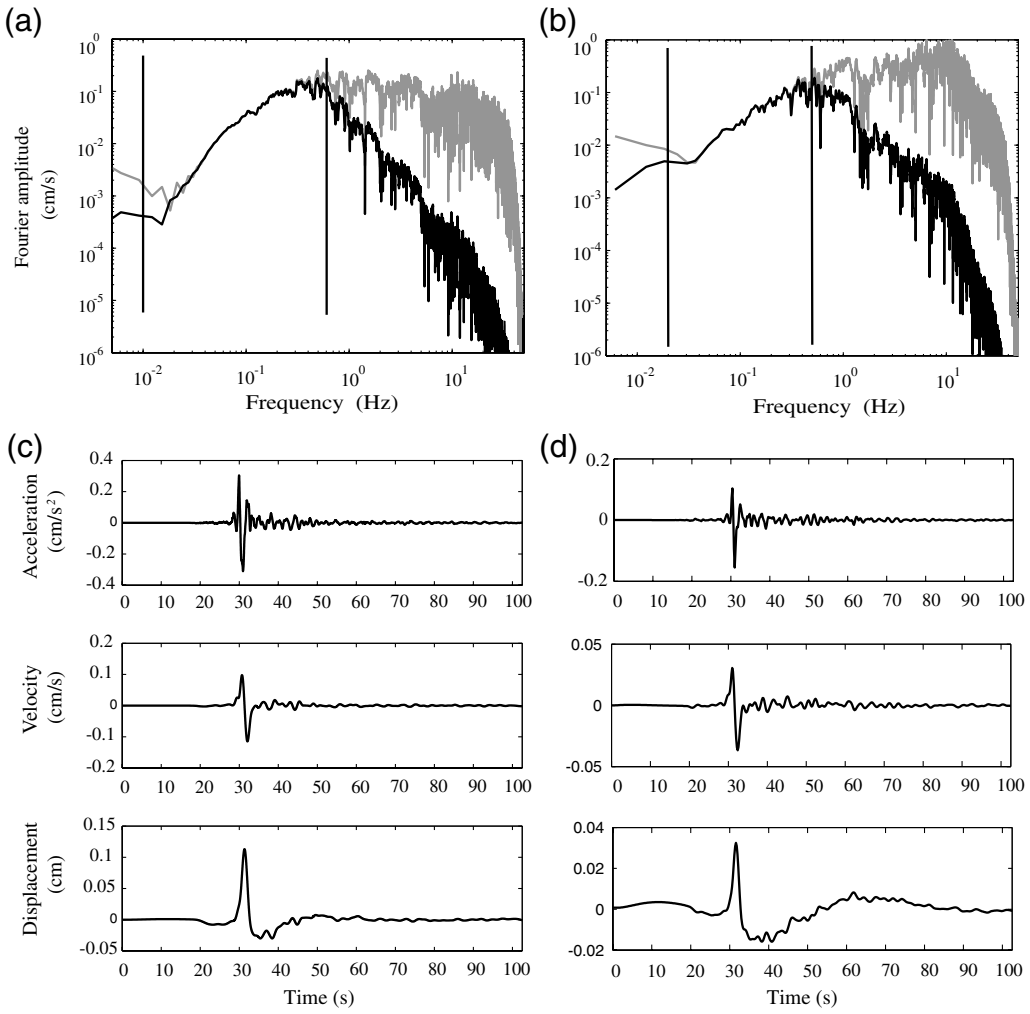

Figure 2. Northern Iwate intermediate depth earthquake of 2008. Fourier spectra of the EW accelerograms recorded at stations (a) IWTH03 and (b) IWT023. The unfiltered spectra are shown in gray; the filtered spectra in black. The band-pass filter had corners of 0.02–0.5 Hz and 0.04–0.5 Hz, respectively. (c) and (d) Filtered acceleration, velocity, and displacement EW records at IWTH03 and IWT023, respectively.

$$D(x,y) = D_m \exp\left[-\left(\frac{x^2}{a^2} + \frac{y^2}{b^2}\right)\right], \qquad (1)$$

where D_m is the maximum amplitude of slip inside the elliptical patch of semi-axes a and b. During the inversion, a constant rupture velocity V_r was assumed. See Table 1 for a list of the parameters we used. A total of seven parameters were inverted; five of these were geometrical: two axes (a, b) and one angle (α), and two for the position of the center of the ellipse. Two additional parameters define the kinematics: the maximum slip D_m and the rupture velocity V_r. The source time function was the same for every point on the fault. By trial and error we chose a triangular function of duration 2 s around the rupture time.

The AXITRA code (Bouchon, 1981; Coutant, 1990) was used to simulate wave propagation from the source to

Table 1
Values of the Seven Inverted Parameters for the Asperity Models Using NA

Model	Semi-Axis a (km)	Semi-Axis b (km)	α (rad)	X (km)	Y (km)	V_r (km/s)	D_m (m)
Dataset 1*	9.02	5.08	0.80	−0.62	0.47	4.31	2.48
Dataset 2*	5.34	5.91	0.08	0.68	0.058	3.24	3.22
Range minimum*	4	4	0	−4	−4	0.1	0.1
Range maximum*	14	14	3.14	4	4	8	10

*The optimal values for the two datasets are on the first two lines, and the range of variation of these parameters during the inversion is shown in the last two lines.

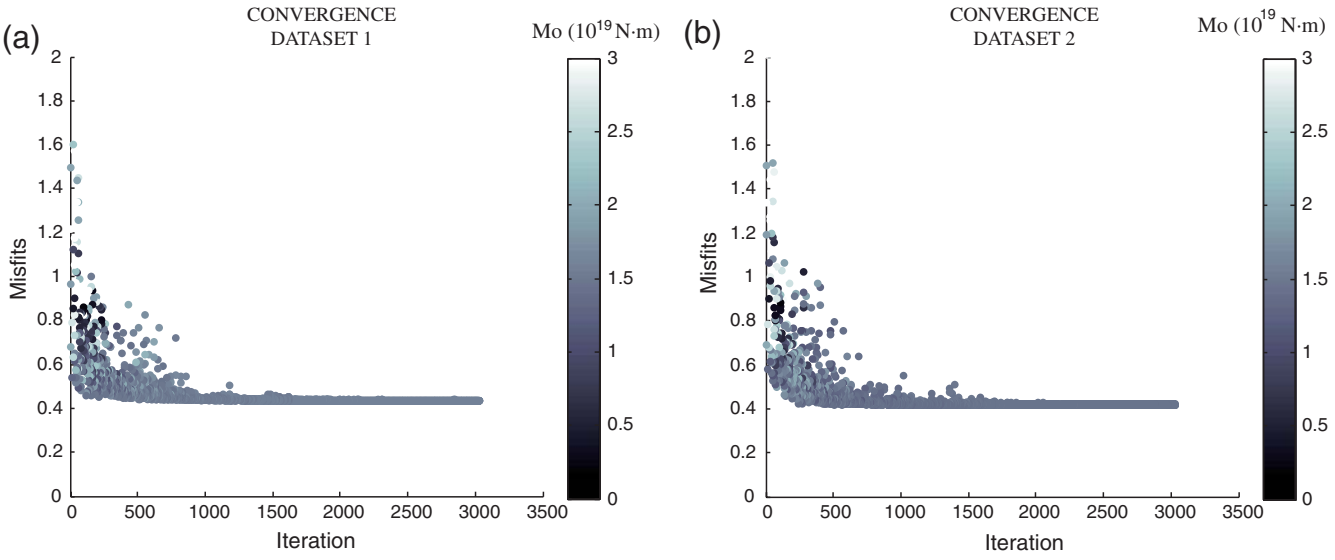

Figure 3. Kinematic inversion of the 2008 Northern Iwate intermediate depth earthquake. The figure shows the misfit between synthetics and observed displacement records as a function of iteration number for the kinematic inversion using NA. Datasets 1 and 2 are shown on (a) and (b), respectively. Each dot is one inversion solution colored by the corresponding seismic moment. The color scale is saturated for $M_0 > 3 \times 10^{19}$ N·m. The solutions converge to a misfit value of 0.436 for Dataset 1 and 0.417 for Dataset 2, and both converge to a moment of $M_0 \approx 1.5 \times 10^{19}$ N·m.

the receivers. For the propagation of seismic waves we used the same model of the structure as Suzuki *et al.* (2009). Their model is a modification of that of Ukawa *et al.* (1984).

The inversion was made using the neighborhood algorithm of Sambridge (1999), to search for the rupture model with minimum misfit, and the Monte Carlo technique, to study the resolution in the vicinity of the best model. Synthetic records were compared with real records using the normalized L^2 norm

$$\chi^2 = \frac{\sum_i (\mathrm{obs}_i - \mathrm{calc}_i)^2}{\sum_i \mathrm{obs}_i^2}, \qquad (2)$$

where obs are the observed displacement and calc, the simulated displacement. The sum runs over all samples in every seismogram considered in the inversion.

Because we disposed of a large number of records, we used different combinations of them to create several datasets. For each dataset, kinematic inversion converged in a few thousand iterations to very similar results. For this reason, we show only the results for two datasets. Dataset 1 consists of 17 KiK-net records filtered between 0.02 and 0.5 Hz, and located within a radius of 65 km from the epicenter; these are denoted by gray and black circles in Figure 1. Dataset 2 consisted of all available K-NET and KiK-net records within 40 km of the epicenter filtered between 0.04 and 0.5 Hz. Dataset 2 is shown by the black circles and squares in Figure 1. Both inversions converge to a well-defined misfit minimum and stable seismic moment close to 1.5×10^{19} N·m in about 3000 iterations as shown in Figure 3. The best models found with the two datasets are listed in Table 1. Figure 4 shows the slip distribution and the rupture isochrones for these two models. In spite of their differences, these models produce very similar records as shown in Figure 5 where we compare observed and synthetic east–west (EW) and north–south (NS) seismograms. The comparison between observed and synthetic records shows a good overall fit of the displacement records except at stations IWTH23, IWTH22, and IWTH04 whose *S*-wave arrival times appear to be shifted with respect to the other records in the dataset. This is probably due to problems with the 1D velocity model.

An important point is how well the synthetics fit the records, not just in time domain, but also in the Fourier spectral domain. In Figure 6 we show two records for the best model obtained from Dataset 1. Full results for both datasets are shown in Ⓔ Figures S1 and S2 (see the electronic supplement to this article). All the synthetic Fourier spectra present a strong negative hole at around 0.5 Hz (the cutoff frequency of the high-pass cutoff filter). This occurs because of negative interference from stopping phases emitted by the edges of the ellipses.

Kinematic Inversion Is Non-Unique

During the study of NA inversions we found different solutions with low misfits. After close examination we found that there was a clear trade-off between maximum slip D_m, rupture velocity V_r, and seismic moment M_0. To explore this trade-off, we did a Monte Carlo inversion of Dataset 1 in which only V_r, D_m, and the semi-axis a were allowed to change. In the MC inversion the semi-axes b and a were forced to have the same aspect ratio ($b/a = 0.56$). This is the aspect ratio for the best model that was found by the NA algorithm. All other parameters were fixed to the values listed in Table 1. In Figure 7 we plot the residuals of the models visited by the MC algorithm; those with misfits lower than

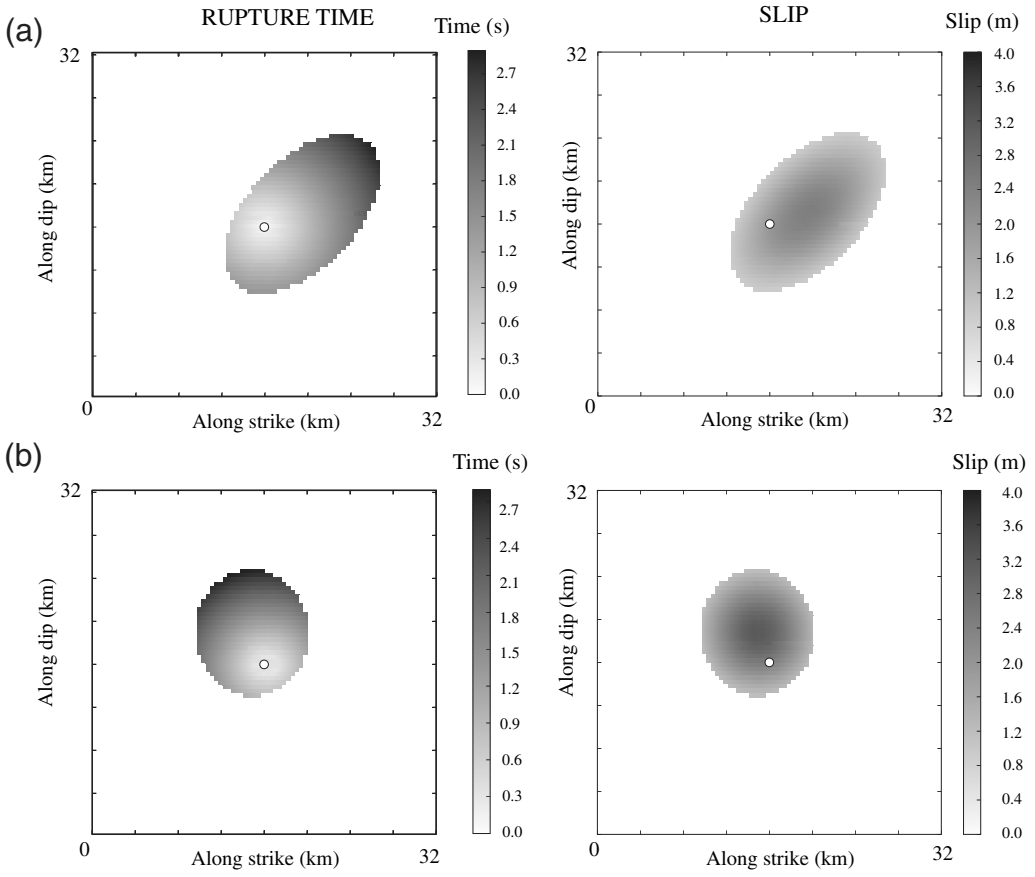

Figure 4. Kinematic inversion of the Northern Iwate intermediate depth earthquake for the best kinematic models of (a) Dataset 1 and (b) Dataset 2. Rupture time isochrones are shown in the left column; slip distribution is show in the right column.

0.5 are plotted with larger dots (50% of the variance is explained by the data). These models preferably fill a zone of the V_r space between 2 and 9 km/s, with D_m from 1 to 8 m and a semi-axis a between 5 and 14 km. The seismic moment M_0 of these models were in the range between 1×10^{19} N·m and 2×10^{19} N·m. The wide range of V_r values observed in Figure 7b,c, includes models with sub-shear and supershear rupture.

This family of solutions provides the overall characteristics of the Iwate earthquake using double-couple mechanism and a single fault plane. These characteristics are in general agreement with the more detailed kinematic study made by Suzuki *et al.* (2009). In Figure 8 we compare the result of the kinematic inversion by Suzuki *et al* (2009) with the best solution we found. In our simulations there are small problems with the NS and vertical components of some records (see Figs. 5 and 6 and Ⓔ Figs. S1 and S2, available in the electronic supplement to this article), which could be due to non-double-couple components in the mechanism (GCMT) or, perhaps, the need for a secondary rupture, as suggested by Suzuki *et al.* (2009).

Dynamic Inversion Method

We did a full dynamic inversion of the near-field strong-motion record starting from the previous kinematic results. We used a single elliptically-shaped fault instead of a grid of rectangles, because the slip discontinuities at the edge of the rectangular patches produce strong stress singularities, and it is not clear how rupture can propagate from one patch to another. It is certainly possible to smooth the stress distribution of the rectangular patches using splines or other interpolation methods. For the moment, however, such an approach is still too expensive because of the large number of degrees of freedom involved. For this reason we adopted the same elliptical-shaped fault model that we used for kinematics assuming that stress and friction were uniform inside the elliptical fault. This is a low frequency approach designed to look for the average properties of the rupture. We assumed that rupture propagation was controlled by the slip-weakening friction law proposed by Ida (1972)

$$T_f(D) = (T_u - T_r)\left(1 - \frac{D}{D_c}\right) + T_r, \qquad (3)$$

where T_f is friction as a function of slip $D(0 < D < D_c)$. T_u is the peak frictional stress or strength, and D_c is the slip-weakening distance. In (3) the constant kinematic or residual friction T_r on the right side cannot be determined from seismic observations only (see Madariaga, 1979). For

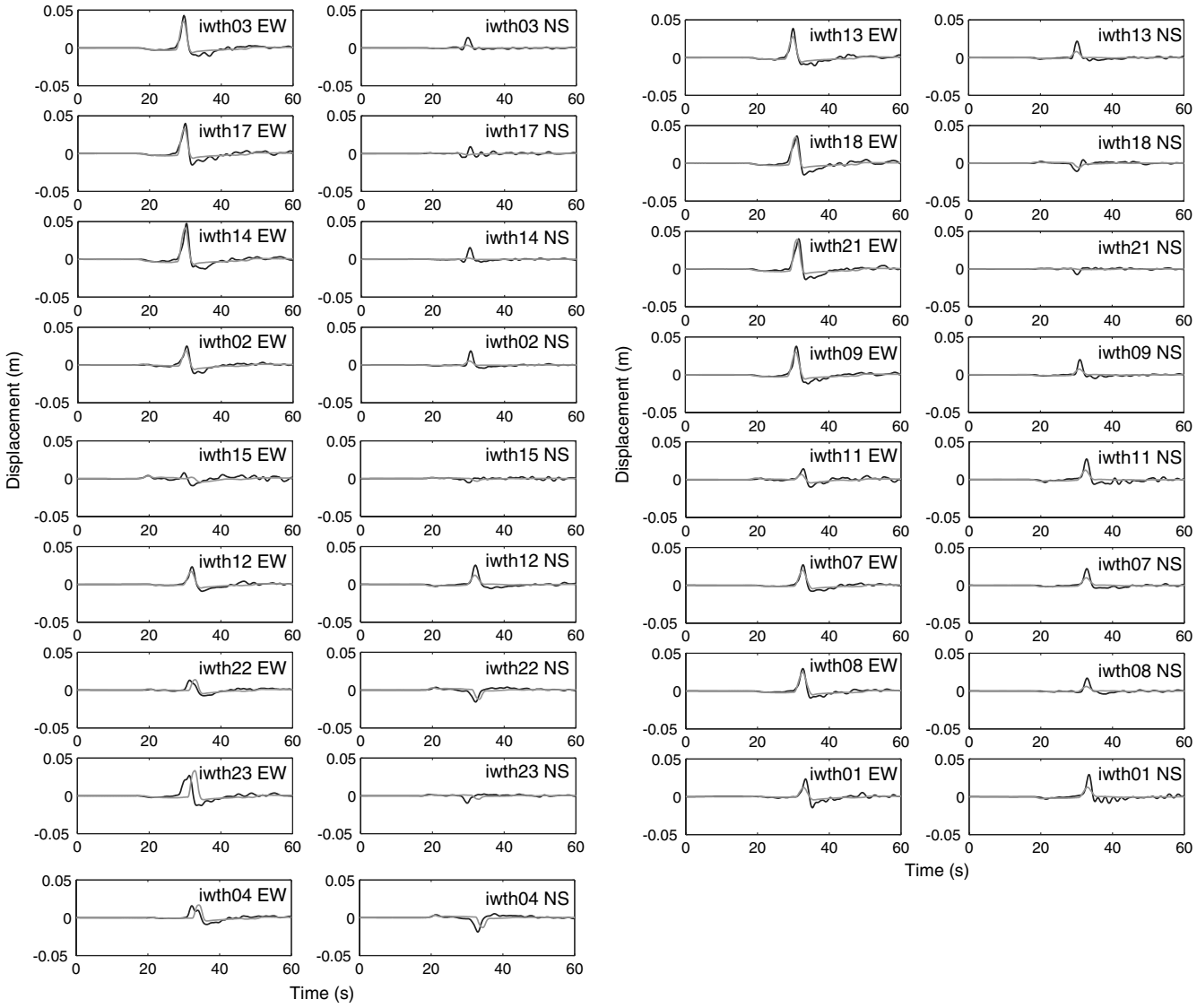

Figure 5. Kinematic inversion of the Northern Iwate intermediate depth earthquake. Comparison of observed (black traces) and synthetic (gray traces) EW and NS displacement records of Dataset 1 for the best kinematic model using NA.

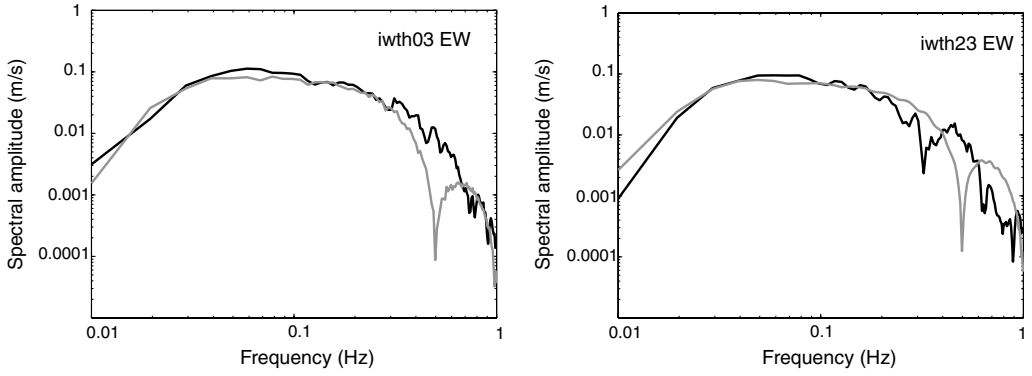

Figure 6. Kinematic inversion of the Northern Iwate intermediate depth earthquake. Comparison of observed data (black) and synthetic record (gray) EW component of Fourier spectra of Dataset 1 for the best model of kinematic inversion using NA.

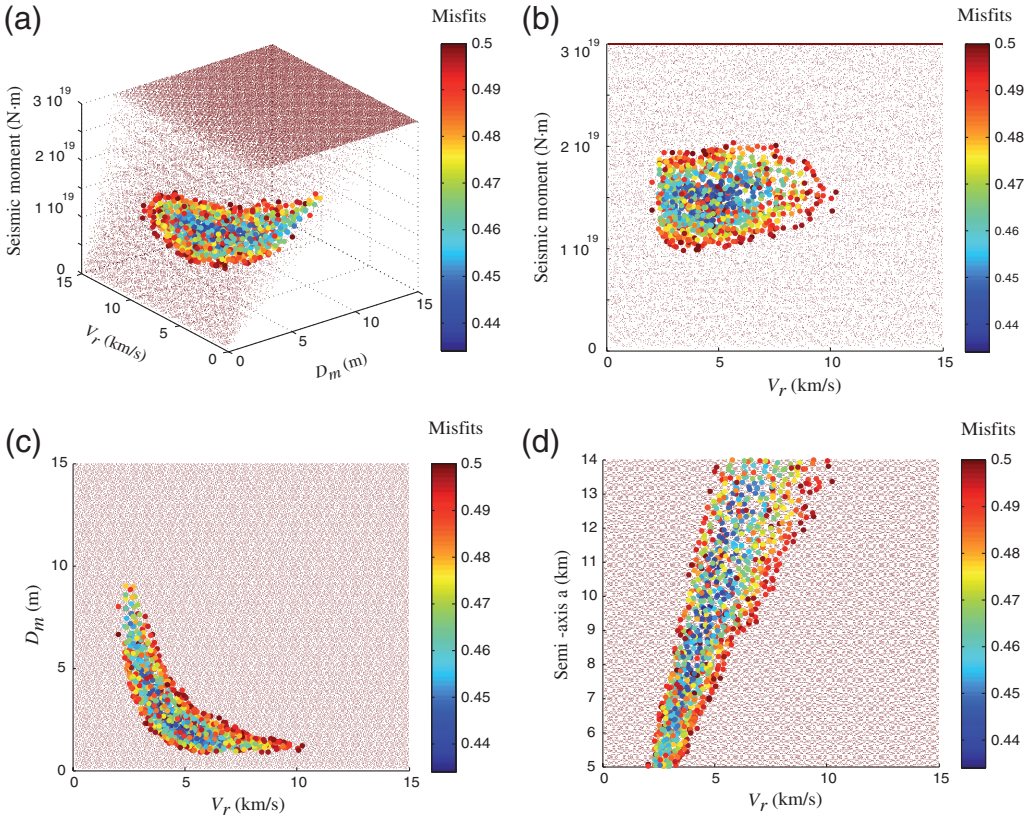

Figure 7. Study of the resolution of the kinematic inversion of the Northern Iwate intermediate depth earthquake by the Monte Carlo method. In each figure, dots plot the result of one simulation. The larger dots have misfits $\chi^2 < 0.5$ and their color is given by the misfit. The color scale is saturated for misfits $\chi^2 \geq 0.5$. (a) Three-dimensional figure showing seismic moment M_0, velocity rupture V_r, and maximum slip D_m; M_0 is saturated for $M_0 > 3 \times 10^{19}$ N·m. (b) Misfits projected on the M_0 versus V_r plane. (c) Misfits projected on the (D_m, V_r) plane. (d) The trade-off between semi-axis a and rupture velocity V_r.

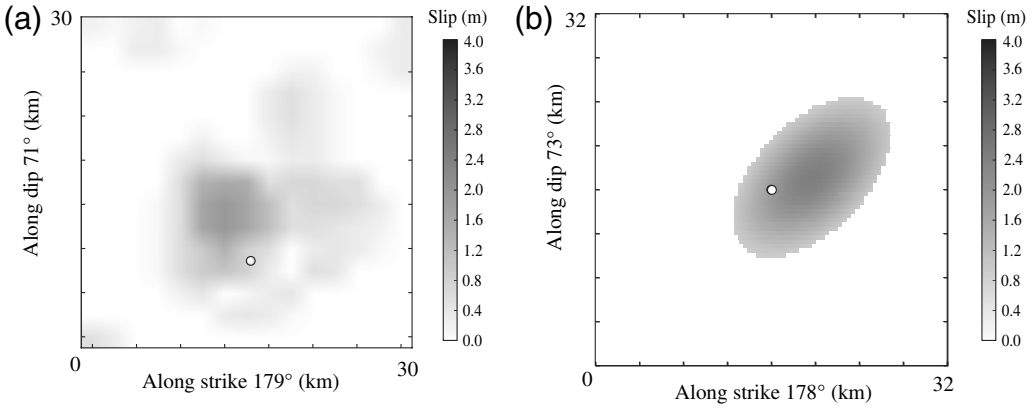

Figure 8. Kinematic inversion of the Northern Iwate intermediate depth earthquake. (a) Slip distribution inverted by Suzuki *et al.* (2009). (b) Slip distribution obtained by kinematic inversion of Dataset 1. The small white dot is the hypocenter.

simplicity, in the following we assume that the residual friction $T_r = 0$. Other, more complex friction laws can be tested, but we do not think that the present data can distinguish them. The only hope for obtaining more detailed friction laws is to go to higher frequencies which, for the moment, are too expensive to model.

In our forward dynamic model, rupture starts at the hypocenter triggered by a small circular asperity following the methodology of Madariaga and Olsen (2000). Once rupture breaks the small asperity, it can grow or stop spontaneously depending on the values of the stress field (T_e) and the friction law. In our model we assumed that stress and friction

were constant inside the elliptical rupture zone. In the dynamic inversion we explored three friction and stress parameters: the yield stress T_u, the slip-weakening distance D_c of the friction law (3) and the external applied stress T_e. Two parameters for the small circular asperity: its radius R' and the stress T'_e that must be higher than the yield stress T_u. In addition, we studied five geometrical parameters: two axes, one angle and the two coordinates of the center of the ellipse. In total, 10 parameters were inverted. As was proposed theoretically by Madariaga (1979), and observed by Ruiz and Madariaga (2011), the seismic data cannot distinguish between barrier (Das and Aki, 1977) or asperity models (Kanamori and Stewart, 1978). For this reason, we only show the inversion made using the asperity model where the region outside the ellipse was considered to have a very large negative initial stress load that was enough to stop rupture when it reached the edge of the ellipse. The stress outside of the ellipse was fixed *a priori* to a very large negative value; we checked that its exact value did not have much influence in the final results as long as it was able to stop rupture.

A 3D fourth-order, staggered-grid finite-differences method with absorbing boundaries and thin fault boundary conditions was used to solve the forward dynamic rupture simulation (Madariaga *et al.*, 1998). The spatial and temporal discretization were 200 m and 0.005 s, respectively. The Courant-Friedrichs-Lewy (CFL) constant for this grid is everywhere less than 0.3 so that the finite-difference method is stable. With this grid size it is possible to model rupture propagation and generate seismograms valid up to the cutoff frequency as we will verify at the end of the dynamic inversion. The grid had $160 \times 160 \times 160$ elements and was centered at the hypocenter on the fault plane. The fault zone is 32 km wide and 32 km deep, but only a small part broke during the earthquake. The AXITRA spectral code was used to simulate wave propagation from the source to the receivers; time and space steps were four times finer than those of the finite-difference grid to ensure accurate simulations. Once we had found the best dynamic model using the NA, we explored a large region around the minimum defined in Table 2 with a Monte Carlo method in order to study the resolution of the inverse problem. As shown by Ruiz and Madariaga (2011), these solutions share the non-dimensional similarity parameter κ

$$\kappa = \frac{(T_e - T_r)^2}{\mu(T_u - T_r)} \frac{L}{D_c}, \tag{4}$$

where L, the characteristic size of the event, is taken as the shorter semi-axis of the source ellipse, μ is the shear modulus. $T_e - T_r$, $T_u - T_r$, and D_c were already defined. As stated above, we assume $T_r = 0$ and we use T_e for $T_e - T_r$ and T_u instead of $T_u - T_r$. κ is roughly the ratio of available strain energy to energy release rate, so that it controls the overall characteristics of the rupture process as discussed by Madariaga and Olsen, (2000).

Dynamic Inversion Results

We carried out non-linear dynamic inversion using the same two datasets we used for kinematic inversion (Fig. 1). Table 2 shows the optimal values for the inverted parameters of the two datasets and the range of values that were explored during the inversion. The best results using NA have a misfit $\chi^2 \approx 0.4$, meaning that our model explains 60% of the observed data. They also converge to a seismic moment $M_0 \approx 1.5 \times 10^{19}$ N·m, similar to that obtained from the kinematic inversion. The misfits for each step in the inversion are shown in Figure 9. In this figure we also show the value of κ for each model using a color scale; κ converges to a value of 1.34 and 1.45 for Dataset 1 and Dataset 2, respectively. The convergence to a well-defined value of κ can be explained by the trade-off between the initial stress and the friction law parameters.

Figure 10 shows the slip distribution and slip rate for the best dynamic models obtained by the NA. The overall characteristics determined by kinematic inversion are confirmed: a very short rupture duration of less than 2.1 s, implying very high sub-shear rupture velocity. Rupture starts in the small asperity and then propagates to the rest of the fault mainly in a direction away from the surface. Figure 11 shows snapshots of slip rate on the fault plotted every 0.4 s. The largest values of slip rate are attained near the boundaries of the ellipse, where the large negative stress stopped the rupture. This happened at about 2.1 s for both datasets.

Figure 12 shows synthetic and observed horizontal displacements at the different sites of Dataset 1. We observe that synthetics reproduce the observed records very well with the exception of those from stations IWTH23, IWTH22, and IWTH04, the same stations that were not well modeled in the kinematic inversion. Duration is in the order of 4–5 s for each record, implying a very fast rupture and a massive stress drop. In Figure 13 we show the Fourier spectra computed

Table 2
Values of the Inverted Parameters

	Geometry					Nucleation		Stress		
Model	Semi-Axis a (km)	Semi-Axis b (km)	Alfa (rad)	X (km)	Y (km)	R' (km)	T'_e (MPa)	T_e (MPa)	T_u (MPa)	D_c (m)
Dataset 1*	4.02	8.06	1.01	0.01	0.06	1.32	61.45	34.25	55.96	1.01
Dataset 2 *	6.77	4.00	0.38	−4.00	−0.90	0.86	83.28	41.15	71.54	1.05
Range minimum *	4	4	0	−4	−4	0.8	8	8	8	0.4
Range maximum *	14	14	1.57	4	4	2	150	50	100	2

*The optimal values are on the first two lines, and the range of variation of these parameters during the inversion are shown in the last two lines.

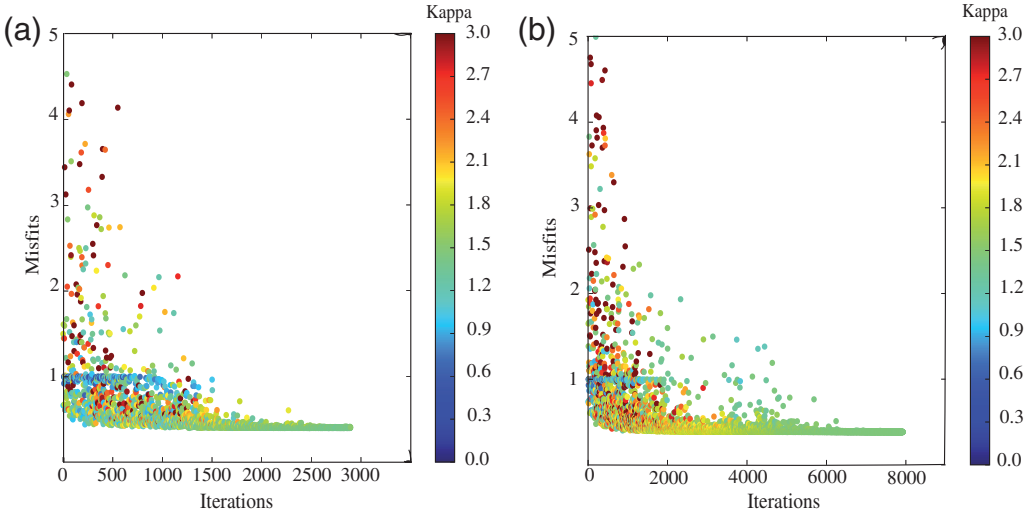

Figure 9. Dynamic inversion of the Northern Iwate intermediate depth earthquake. Misfit between synthetics and observed displacement records as a function of iteration number for Datasets (a) 1 and (b) 2. The solutions converge to misfit values of 0.39 for Dataset 1 and 0.38 for Dataset 2. The color corresponds to the value of κ computed for each model. The color scale is saturated for $\kappa > 3$; κ converges to 1.34 for Dataset 1 and 1.44 for Dataset 2.

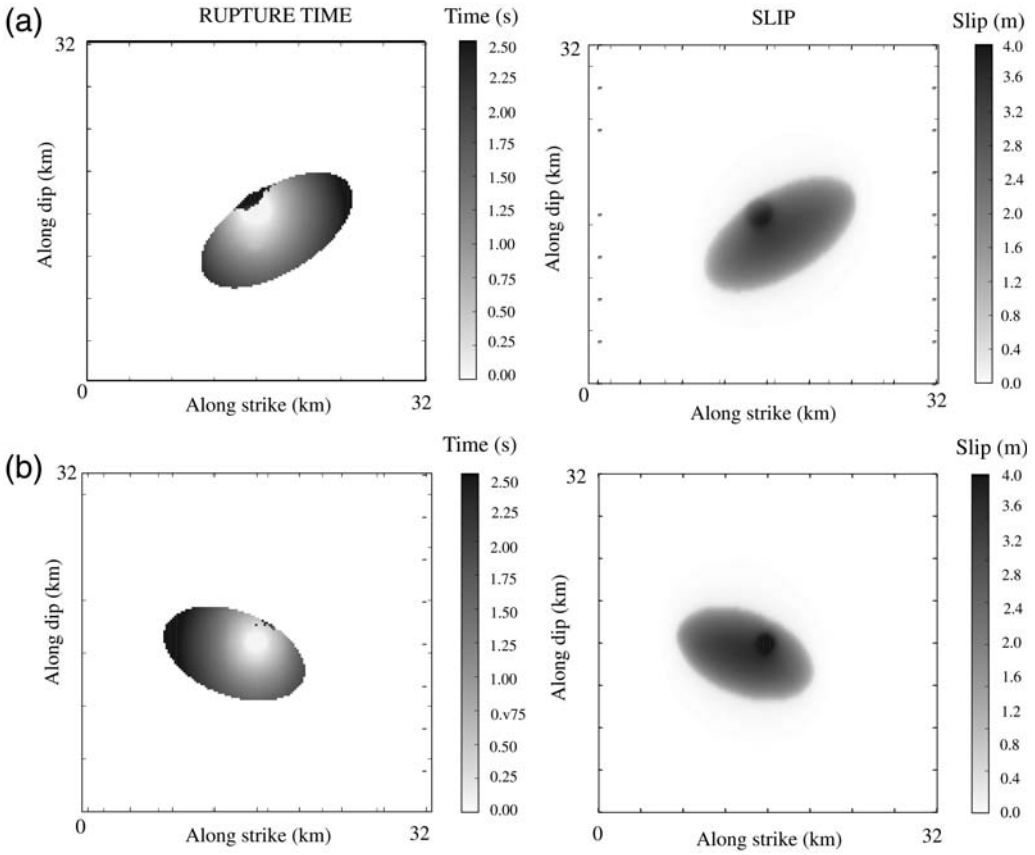

Figure 10. Dynamic inversion of the Northern Iwate intermediate depth earthquake. Rupture isochrones and slip distribution for (a) Dataset 1 and (b) Dataset 2.

for a subset of the EW components of the seismograms shown in Figure 12. We observe that the dynamic models fit the spectra much better than the kinematic models shown in Figure 5. The most obvious difference is that the spectral hole near 0.5 Hz is only present in some of the most distant stations. We think that this is an effect of the variable rupture speed of dynamic models. In Ⓔ Figure S3 (see the electronic supplement to this article) we show all the components of

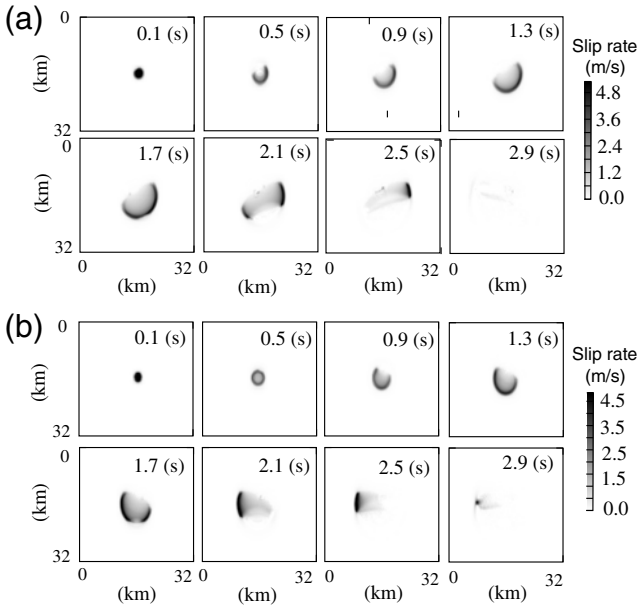

Figure 11. Dynamic inversion of the Northern Iwate intermediate depth earthquake. Snapshots of slip rate for the best model obtained by dynamic inversion of (a) Dataset 1 and (b) Dataset 2.

Dataset 1, and in Ⓔ Figure S4 (see the electronic supplement to this article) we show the results for Dataset 2.

Dynamic Inversion Is Non-Unique

The previous results show that dynamic models converge to a zone where the misfit is of the order of 0.38–0.39 and the value of parameter κ approaches 1.34–1.45. There is a clear trade-off between κ and the fit χ of the seismograms. This trade-off implies that there must be several models with similar κ that fit the data with a certain misfit. In order to explore the resolution of dynamic inversion, we used the Monte Carlo method, fixing the geometric parameters to be those of the best dynamic model found from the inversion of Dataset 1. The parameters for this model are listed in Table 2. Because the exploration of the model space is expensive and difficult to plot, we decided to explore values of the dynamic parameters T_e, T_u, and D_c, keeping all other parameters fixed to those of the best model. In Figure 14a we plot the results of Monte Carlo exploration in the space of dynamic parameters T_e, T_u, and D_c. The fit of each model to the observed data is shown with the color scale. Models plotted in brown correspond to a combination of stress-friction parameters that produce models that do not fit the data at all, many having misfits χ^2 larger than 1. Models with misfits lower than 0.5 are drawn with large blue dots; these dots represent a family of models that fit the observations well. The results are similar to those observed for the Michilla 2007 inversion (Ruiz and Madariaga, 2011). The models that have lower misfits are located on a relatively flat irregular surface in the space of parameters T_e, T_u, and D_c (Fig. 14a). The zone is elongated in the T_u, D directions. We already observed, in Figure 8, that convergence was closely related to the value of κ. In Figure 12 we projected the results onto the plane (T_e^2, $T_u D_c$). We observe (Fig. 14b) that the blue models, those that have misfits less than 50%, are now located in a narrow wedge; this means that the good models are controlled by the ratio of T_e^2 to $T_u D_c$.

Finally, we plotted the seismic moment M_0 of the models against their κ. All the models that fit the data with error less than 50% are now grouped in an elongated area where the seismic moment varies around 1.5×10^{19} N·m and κ varies between 1 and 2.5. As was proposed by Madariaga and Olsen (2000), large values of κ correspond to models that tend to propagate at supershear velocities. Considering that more than 30,000 models were visited during the MC inversion, the number of supershear models that fit the data is small but not null. Among these models, we chose one with low misfit ($\chi^2 = 0.45$) and high value of kappa ($\kappa = 2.06$). The parameters T_e, T_u, and D_c for this model are listed in Table 3. Although the synthetic records are very similar to those computed for sub-shear ruptures (see Ⓔ Fig. S5, available in the electronic supplement to this article), the rupture process for the supershear model is very different from that of the model with best fit. In Figure 15 we show the slip and rupture isochrones for the supershear event. The rupture front shown in Figure 15a presents a clear supershear instability in the in-plane direction which for the Iwate intermediate depth earthquake is in the almost vertical direction. The rupture front at 1 s has the characteristic "ears" in the supershear direction (see Fig. 16c). The jump to supershear speed occurred around 0.7 s.

Discussion

The kinematic and dynamic inversion of the 2008 Northern Iwate intermediate depth earthquake are non-unique even if the sources are described by simple elliptical patches. In the kinematic inversion, the solutions collapse to a limited set of values of rupture velocity, maximum slip, and area of the ellipse, which converge to the similar values of the seismic moment of 1.5×10^{19} N·m and duration of the earthquake. Figure 16a shows snapshots of slip-rate at regular intervals of 1 s for the best model obtained by kinematic inversion of Dataset 1. The rupture process is strongly controlled by assumed rise time of 2 s. We tried other rise times but they could not be resolved, because the observed and synthetics are low-pass filtered at 0.5 Hz.

Figure 16 compares the slip-rate of (a) the best model found by kinematic inversion, (b) the best model obtained by dynamic inversion, and (c) the supershear dynamic solution obtained using Dataset 1. The kinematic solution differs with respect to the dynamic solution especially because rupture is up-dip for kinematic models and down-dip for dynamic inversion. We think that seismic ruptures obtained by kinematic and dynamic inversion do not necessarily agree with respect to rupture propagation. Figures 6 and 7, and Ⓔ Figures S1, S2, S3, and S4 (see the electronic supplement

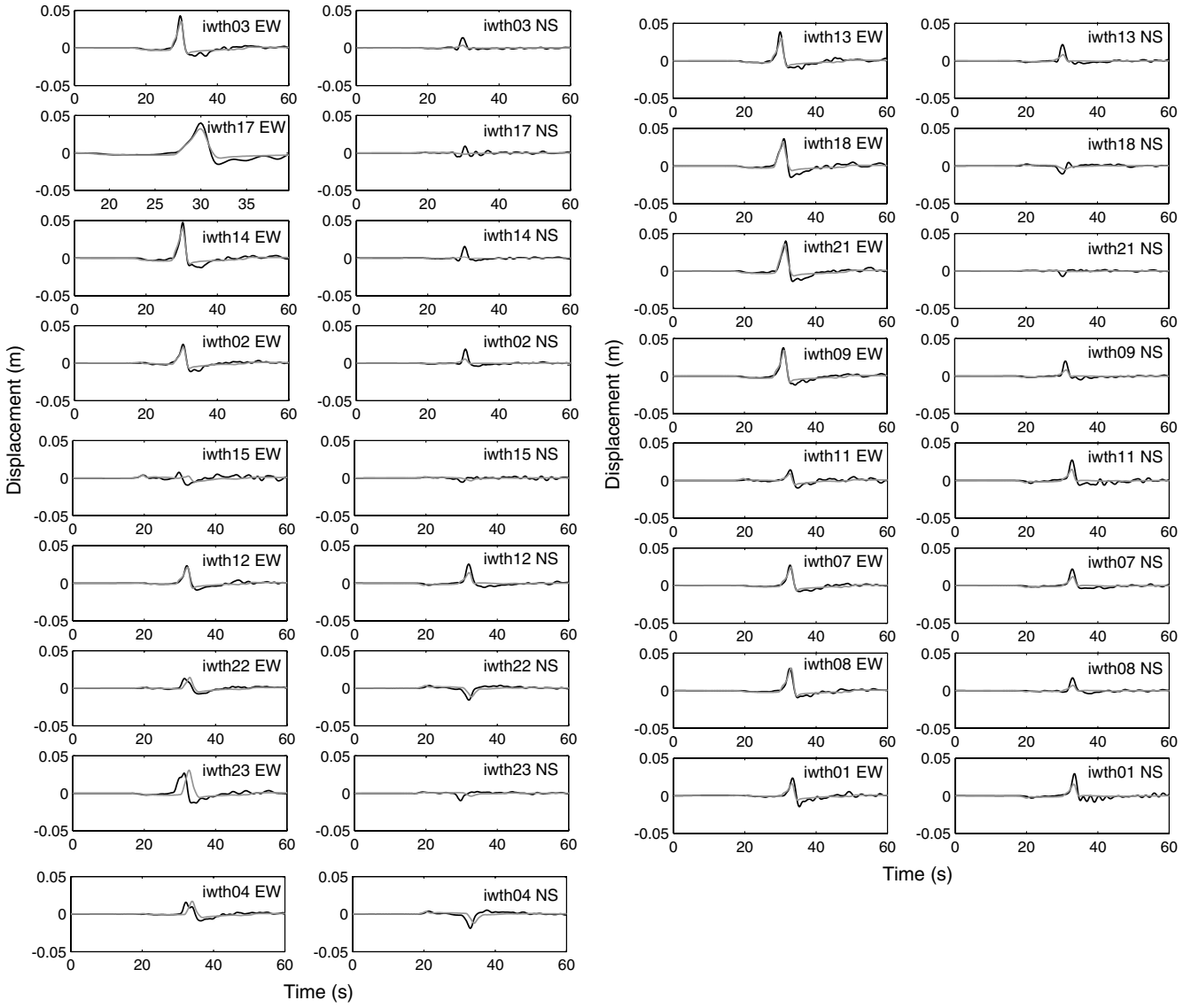

Figure 12. Dynamic inversion of the Northern Iwate intermediate depth earthquake of Dataset 1. Comparison of the EW component of the observed displacements (black) with the synthetics (gray) computed for the best dynamic model obtained by dynamic inversion.

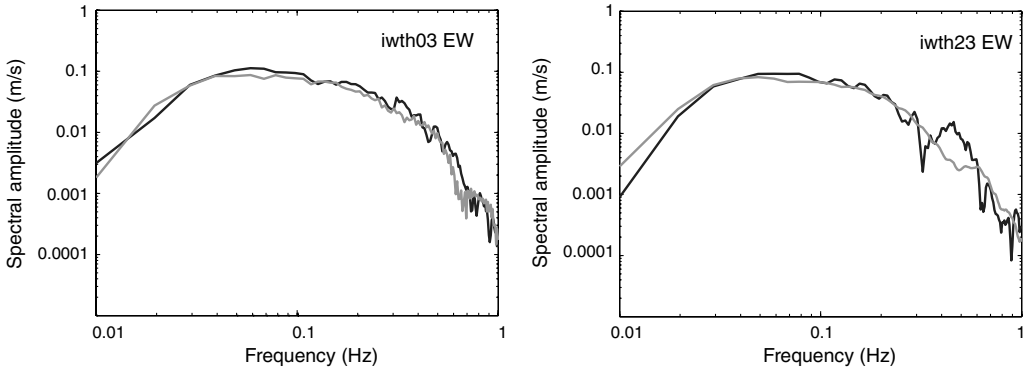

Figure 13. Dynamic inversion of the Northern Iwate intermediate depth earthquake. Comparison of observed spectra (black) and the Fourier spectra of the computed displacement records (gray) for the best model found by dynamic inversion of Dataset 1.

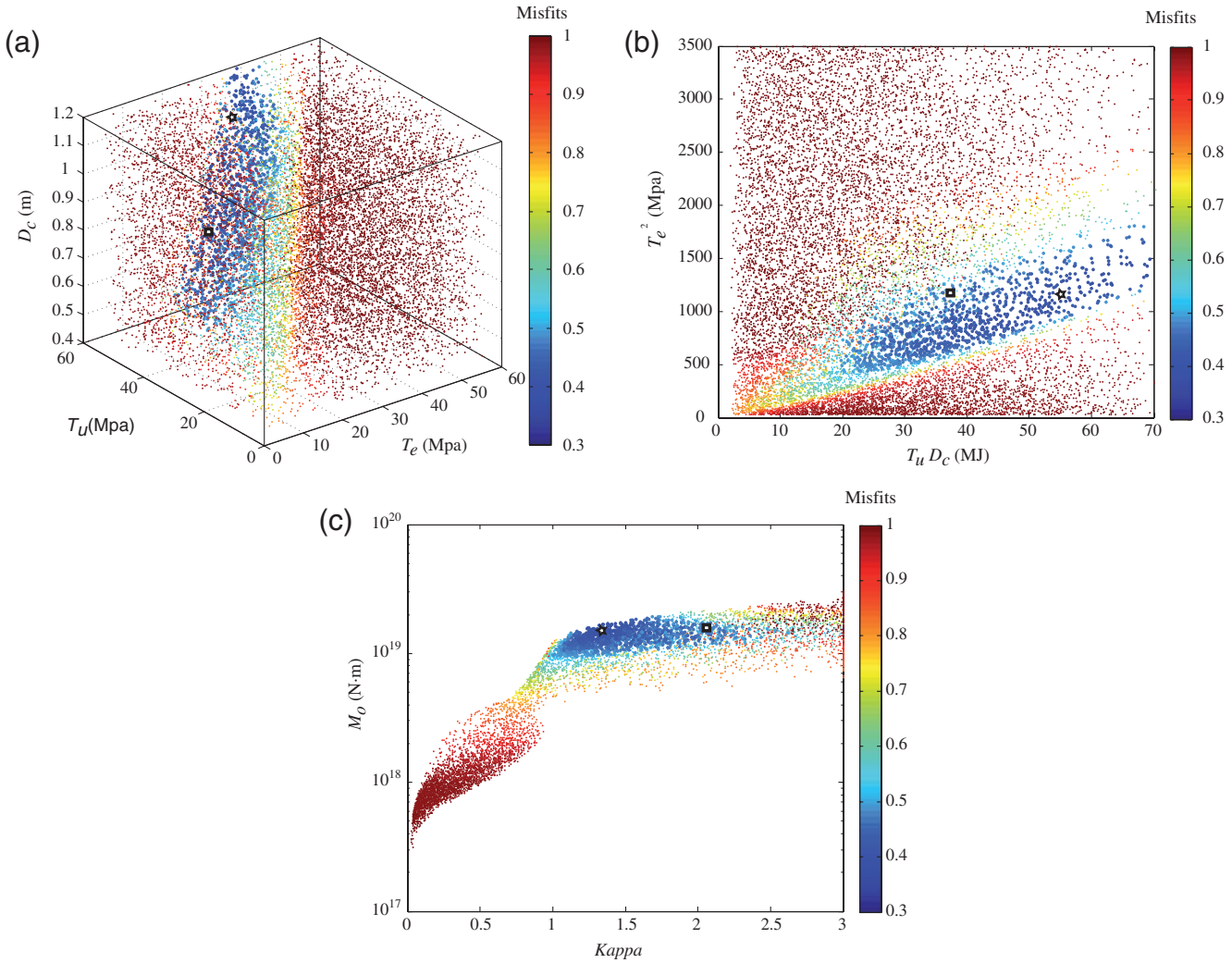

Figure 14. Dynamic inversion of the 2008 Northern Iwate intermediate depth earthquake. Each dot represents a model; the dots are colored by the misfit value following the color scale shown on the right. The scale is saturated for misfits ≥0.5. (a) Plot of misfits for each model projected onto the space of dynamic parameters T_e, T_u, and D_c. (b) Projection of model space onto the plane T_e^2 and $T_u D_c$. The misfits lower than 0.5 converge to a narrow band. (c) Projection of model space onto the plane M_0 and κ. The misfits lower than 0.5 are controlled by the seismic moment ($M_0 \sim 1.5 \times 10^{19}$ N·m) and a narrow band of k values ($1 \leq \kappa \leq 1.6$). The black star corresponds to the optimal solution determined by NA, and the black square is the supershear solution shown in Figure 15.

to this article) show that kinematic inversions do not reproduce high frequency waves as well as dynamic inversions. In spite of this difference, the synthetic seismograms computed for the best models obtained by kinematic and dynamic inversions are very similar, as shown in Ⓔ Figure S6 (see the electronic supplement to this article).

The admissible solutions from dynamic inversion form a region in parameter space that is controlled by the dynamic similarity parameter κ and the seismic moment. As shown by Madariaga and Olsen (2000), κ is a measure of the ratio between strain energy release per unit surface and the specific energy release rate, which in turn control rupture propagation. We can be more specific for the models shown in Figure 14c. These models share the same elliptical geometry described by the first line of Table 2; thus, they all have the same ellipticity $\varepsilon = a/b = 2$. The slip on an elliptical fault under constant stress drop can be computed using equation (10) from Madariaga (1979). The strain energy release for such a fault is simply

$$\Delta W = \frac{2}{3} C_f \frac{T_e^2}{\mu} \pi a^2 b, \tag{5}$$

where a, b are the length of the semi-axes, and C_f is a form factor. For an ellipse of ellipticity 2, we find, from figure 1 of

Table 3
Parameters for a Possible SuperShear Model of the 2008 Northern Iwate Intermediate Depth Earthquake

χ^2	κ	M_0 (N·m)	T_e (MPa)	T_u (MPa)	D_c (m)
0.45	2.06	1.59×10^{19}	34.83	59.78	0.63

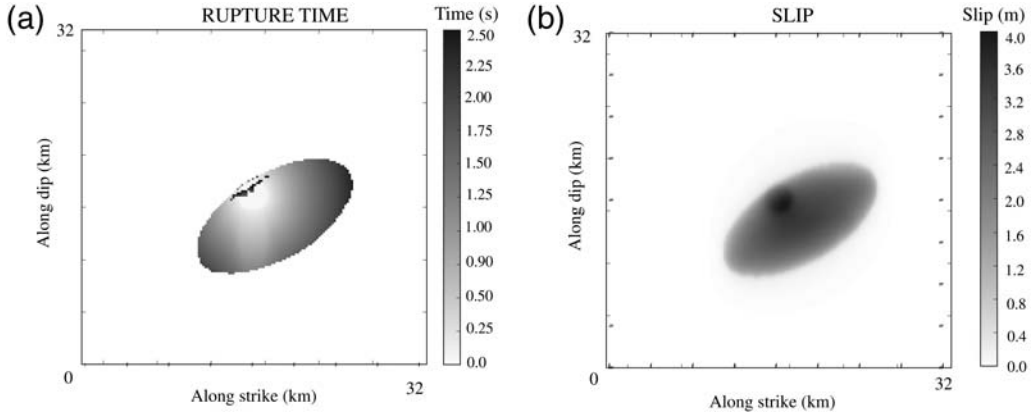

Figure 15. (a) Rupture isochrones and (b) slip of model with supershear rupture for the 2008 Iwate earthquake of northern Japan.

Madariaga (1979), that $C_f \approx 1.35$. We can also calculate the total fracture energy used to propagate the fault, $G_c S$, where the energy release rate for the friction model (3) is $G_c = 1/2 T_u D_c$ times the surface of the fault. The ratio of energy release to fracture energy is thus

$$\frac{\Delta W}{G_c S} = 1.8\kappa. \tag{6}$$

Looking at Figure 14c we observe that only solutions with $\kappa > 1$ fit the data so that the critical value of κ_c for the dynamic inversion of the Northern Iwate earthquake is of the order of 0.98. This is the boundary that separates rupture models that do not propagate from models that break the entire fault. As κ increases beyond the critical value, ruptures propagate at increasingly faster speeds; and for values of $\kappa > 1.5\kappa_c$ supershear solutions become possible. The model of Table 3 with $\kappa = 2.06$ is an example (see Madariaga and Olsen, 2000 for further discussion).

The preferred models of the Iwate 2008 earthquake are ellipses with semiminor axes close to 4 km and have maximum slip of 4 m. Rupture duration for the two best models of Table 2 were less than 3 s and propagated at high subshear velocities. The stress drop T_e obtained from dynamic inversion of the Northern Iwate earthquake is very high, on the order of 30–40 MPa. These T_e values are in agreement with those determined for other intraslab intermediate depth events in Japan, like the 1993 Kushiro-oki earthquake (Takeo *et al.*, 1993; Ide and Takeo, 1996). In general, the results are also similar to those obtained for another intraslab intermediate depth earthquake of similar magnitude, the Michilla 2007 Northern Chile earthquake (Ruiz and Madariaga, 2011). The energy release rate can be computed from $G_c = 1/2 T_u D_c$. It is 23 MJ/m^2 for Dataset 1 and 36 MJ/m^2 for Dataset 2. These are large values compared with values of G_c estimated for similar magnitude events by Abercombrie and Rice (2005) and for subduction events in northern Chile by Lancieri *et al.* (2012). These large values of G_c indicate that rupture propagation at intermediate depths requires much more energy than it does in shallow events.

For these intermediate depth events, an elliptical rupture provides an efficient model of the event that can be inverted with present-day computational resources. More complex source models, including variations of slip and stress on the fault plane, are the next step in dynamic inversion. Larger magnitude earthquakes, or more complex ruptures, may also be modeled using more than one ellipse as was done for the 2000 Tottori, Japan, earthquake by Di Carli *et al.* (2010).

Conclusions

We applied an elliptical patch approach to do kinematic and dynamic inversion of the intermediate depth 2008 Iwate earthquake. We explored the solution space in order to find the overall characteristics of the seismic rupture in the frequency band from 0.02 to 0.5 Hz. We used displacement waveforms obtained by integration of the strong-motion records from the KiK-net and K-NET networks. We obtained excellent fits of the displacement time series, and Fourier spectra show that we fit the entire frequency band of the filtered records. Both dynamic and kinematic inversions are non-unique with large trade-offs between the control parameters. For the dynamic inversion we found that models that fit the data with similar errors can be described with similar values of seismic moment M_0 and dynamic similarity κ. These are two global parameters that describe the size of the earthquake (M_0) and the ratio of strain to fracture energy for the event (κ). It would be tempting to reformulate the results in terms of the radiation efficiency, the ratio between radiated energy and available strain energy that can be derived from κ, but our model does not include high frequencies. We conclude, conservatively, that dynamic inversion using the elliptical patch approximation gives results that are in excellent agreement with simpler dynamic models of seismic radiation, like the Brune-Aki scaling laws. In the future, we will try to evaluate radiated energy more accurately.

Data and Resources

The strong-motion data used in this study were collected from the NIED in Japan. Data can be obtained from the K-NET

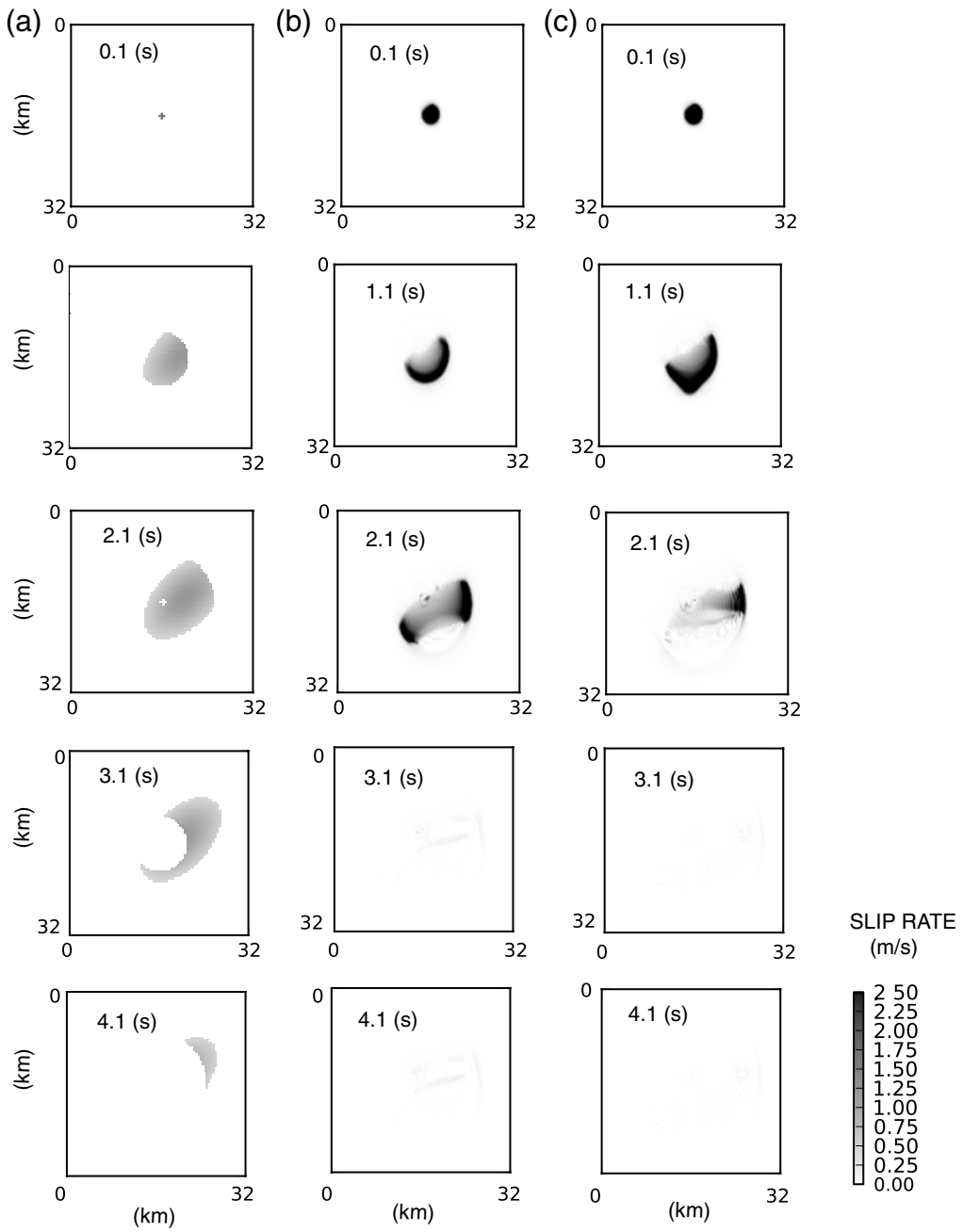

Figure 16. Snapshots show slip rate on the fault. They are shown at four successive instants of time at one second intervals. (a) The best model obtained by kinematic inversion; (b) the best model determined by dynamic inversion; (c) the supershear dynamic solution obtained using Dataset 1.

and KiK-net websites at http://www.k-net.bosai.go.jp/ (last accessed June 2012) and http://www.kik.bosai.go.jp (last accessed June 2012). The Global Centroid Moment Tensor (GCMT) Project database was searched using http://www.globalcmt.org/CMTsearch.html (last accessed September 2012).

Acknowledgments

This work is part of the Millennium Nucleus Program "Montessus de Ballore—IERC" of Mideplan, Chile. Funding for this work was provided by contract FONDECYT Number 1100429 in Chile and by contract DEBATE of ANR Risk-08 and DYNTOHOKU of ANR Flash Japon in France. We thank Michel Bouchon and two anonymous reviewers for their very useful and constructive reviews. We are especially indebted to a reviewer that pointed out to us that the best kinematic and dynamic models propagated in opposite directions.

References

Abercrombie, R. E., and J. R. Rice (2005). Can observations of earthquake scaling constrain slip weakening? *Geophys. J. Int.* **162,** 406–424.

Aoi, S., K. Obara, S. Hori, K. Kasahara, and Y. Okada (2000). New strong-motion observation network: KiK-net, *Eos Trans. AGU* **329**.

Bouchon, M. (1981). A simple method to calculate Green's functions for elastic layered media, *Bull. Seismol. Soc. Am.* **71,** 959–971.

Bouchon, M., M. Campillo, and F. Cotton (1998). Stress field associated with the rupture of the 1992 Landers, California, earthquake and its implication concerning the fault strength at the onset of the earthquake, *J. Geophys. Res.* **103,** 21,091–21,097.

Coutant, O. (1990). Programme de simulation numerique AXITRA, *Rapport LGIT* Université Joseph Fourier, Grenoble, France.

Das, S., and K. Aki (1977). Fault plane with barriers-versatile earthquake model, *J. Geophys. Res.* **82,** no. B36, 5658–5670.

Di Carli, S., C. Francois-Holden, S. Peyrat, and R. Madariaga (2010). Dynamic inversion of the 2000 Tottori earthquake based on elliptical subfault approximations, *J. Geophys. Res.* **115,** B12328, doi: 10.1029/2009JB006358.

Fukuyama, E. (1991). Inversion for the rupture details of the 1987 East Chiba earthquake, Japan, using a fault model based on the distribution of relocated aftershocks, *J. Geophys. Res.* **96,** no. B5, 8205–8217

Fukuyama, E., and T. Mikumo (1993). Dynamic rupture analysis: Inversion for the source process of the 1990 Izu Oshima, Japan earthquake (M 6.5), *J. Geophys. Res.* **88,** 6529–6542.

Guatteri, M., and P. Spudich (2000). What can strong-motion data tell us about slip-weakening fault friction laws? *Bull. Seismol. Soc. Am.* **90,** 98–116.

Ida, Y. (1972). Cohesive force across tip of a longitudinal-shear crack and Griffith specific surface-energy, *J. Geophys. Res.* **77,** 3796–3805.

Ide, S., and M. Takeo (1996). The dynamic rupture process of the 1993 Kushiro-oki earthquake, *J. Geophys. Res.* **101,** 5561–5675.

Kanamori, H., and G. S. Stewart (1978). Seismological aspects of the Guatemala earthquake of February 4, 1976, *J. Geophys. Res.* **83,** 3427–3434.

Kikuchi, M., and H. Kanamori (1995). The Shikotan earthquake of October 4, 1994: Lithospheric earthquake, *Geophys. Res. Lett.* **22,** 1025–1028.

Kinoshita, S. (1998). Kyoshin net (K-NET), *Seismol. Res. Lett.* **69,** 209–332.

Lancieri, M., R. Madariaga, and F. Bonilla (2012). Spectral scaling of the aftershocks of the Tocopilla 2007 earthquake in northern Chile, *Geophys. J. Int.* **189,** 469–480.

Madariaga, R. (1979). On the relation between seismic moment and stress drop in the presence of stress and strength heterogeneity, *J. Geophys. Res.* **84,** 2243–2250.

Madariaga, R., and K. B Olsen (2000). Criticality of rupture dynamics in 3-D, *Pure Appl. Geophys.* **157,** 1981–2001.

Madariaga, R., K. B. Olsen, and R. Archuleta (1998). Modeling dynamic rupture in a 3D earthquake fault model, *Bull. Seismol. Soc. Am.* **88,** 1182–1197.

Miyatake, T., Y. Yagi, and T. Yasuda (2004). The dynamic rupture process of the 2001 Geiyo, Japan, earthquake, *Geophys. Res. Lett.* **31,** L12612, doi: 10.1029/2004GL019721.

Okada, T., and A. Hasegawa (2003). The M 7.1 May 26, 2003 off-shore Miyagi Prefecture Earthquake in northeast Japan: Source process and aftershock distribution of an intra-slab event, *Earth Planets Space* **55,** 731–739.

Peyrat, S., and K. B. Olsen (2004). Nonlinear dynamic rupture inversion of the 2000 Western Tottori, Japan, earthquake, *Geophys. Res. Lett.* **31,** L05604, doi: 10.1029/2003GL019058.

Piatanesi, A., E. Tinti, M. Cocco, and E. Fukuyama (2004). The dependence of traction evolution on the earthquake source time function adopted in kinematic rupture models, *Geophys. Res. Lett.* **31,** L04609, doi: 10.1029/2003GL019225.

Ruiz, S., and R. Madariaga (2011). Determination of the friction law parameters of the M_w 6.7 Michilla earthquake in northern Chile by dynamic inversion, *Geophys. Res. Lett.* **38,** L09317, doi: 10.1029/2011GL047147.

Sambridge, M. (1999). Geophysical inversion with a Neighbourhood Algorithm -I. Searching a parameter space, *Geophys. J. Int.* **138,** 479–494.

Suzuki, W., S. Aoi, and H. Sekiguchi (2009). Rupture process of the 2008 northern Iwate intraslab earthquake derived from strong-motion records, *Bull. Seismol. Soc. Am.* **99,** 2825–2835, doi: 10.1785/0120080331.

Takeo, M., S. Ide, and Y. Yoshida (1993). The 1993 Kushiro-oki, Japan, earthquake: A high stress-drop event in a subducting slab, *Geophys. Res. Lett.* **20,** 2607–2610.

Ukawa, M., M. Ishida, S. Matsumura, and K. Kasahara (1984). Hypocenter determination method of the Kanto-Tokai observational network for microearthquakes, *Rep. Nat'l. Res. Disaster Prev.* **53,** 1–88 (in Japanese with English abstract).

Departamento de Geología
Universidad de Chile
Blanco Encalada 2002
Santiago, Chile
sruiz@ing.uchile.cl
(S.R.)

Laboratoire de Géologie
Centre National de la Recherche Scientifique
École Normale Supérieure
24 Rue Lhomond
75231 Paris Cedex 05, France
madariag@geologie.ens.fr
(R.M.)

Manuscript received 16 February 2012